

The eccentricity in heavy-ion collisions from Color Glass Condensate initial conditions

Azfar Adil,¹ Hans-Joachim Drescher,² Adrian Dumitru,³ Arata Hayashigaki,³ and Yasushi Nara³

¹ Physics Department, Columbia University, 538 West 120th Street, New York, NY 10027, USA

² Frankfurt Institute for Advanced Studies (FIAS), Johann Wolfgang Goethe-Universität,
Max-von-Laue-Str. 1, 60438 Frankfurt am Main, Germany

³ Institut für Theoretische Physik, Johann Wolfgang Goethe-Universität,
Max-von-Laue-Str. 1, 60438 Frankfurt am Main, Germany

The eccentricity in coordinate-space at midrapidity of the overlap zone in high-energy heavy-ion collisions predicted by the k_\perp -factorization formalism is generically larger than expected from scaling with the number of participants. We provide a simple qualitative explanation of the effect which shows that it is not caused predominantly by edge effects. We also show that it is quite insensitive to “details” of the unintegrated gluon distribution functions such as the presence of leading-twist shadowing and of an extended geometric scaling window. The larger eccentricity increases the azimuthal asymmetry of high transverse momentum particles. Finally, we point out that the longitudinal structure of the Color Glass Condensate initial condition for hydrodynamics away from midrapidity is non-trivial but requires understanding of large- x effects.

PACS numbers: 12.38.Mh,24.85.+p,25.75.Ld,25.75.-q

I. INTRODUCTION

Elliptic flow [1] – the azimuthal momentum anisotropy of produced particles with respect to the reaction plane, $v_2 = \langle \cos(2\phi) \rangle$ – is one of the key observables for collective behavior in heavy ion collisions. The large v_2 observed experimentally in semi-central Au+Au collisions at the Relativistic Heavy-Ion Collider (RHIC) [2] is consistent with non-viscous hydrodynamic expansion of a quark gluon plasma (QGP) droplet [3]. On the other hand, a hadron “plasma” with small transverse pressure as initial condition underestimates v_2 at midrapidity [4]. These observations have been interpreted as an indication for the formation of a QGP with very small viscosity shortly after the instant of collision.

Specific solutions of partial differential equations such as hydrodynamics in general depend on the assumed boundary conditions. Here, we focus on the initial conditions for the subsequent evolution of the matter created in non-central Au+Au collisions at RHIC. Specifically, we consider the “Color Glass Condensate” (CGC) initial conditions within a k_\perp -factorization approach [5].

The elliptic flow v_2 in the final state is proportional to the initial spatial eccentricity ε in the plane $\mathbf{r}_\perp = (r_x, r_y)$ perpendicular to the beam axis,

$$\varepsilon = \frac{\langle r_y^2 - r_x^2 \rangle}{\langle r_y^2 + r_x^2 \rangle}. \quad (1)$$

The average is taken with respect to the initial energy density distribution. The reaction plane is spanned by the beam (z) and impact parameter (x) directions.

Ref. [6] observed that the CGC initial conditions correspond to much larger eccentricity than the commonly assumed scaling of the initial energy density with the local number of participants. In fact, hydrodynamical simulations with such initial conditions were shown to overestimate the measured v_2 even if dissipative effects

in the cool hadronic phase are taken into account (by using a hadronic cascade [7] rather than hydrodynamics). However, ref. [6] argued that the different eccentricities obtained from the CGC and Glauber model, respectively, arise from mainly the low-density edges of the overlap region where the CGC approach is less trustworthy.

In this paper we show that more sophisticated models for the nuclear unintegrated gluon distribution $\phi(x, k_\perp)$ than those employed in the original KLN approach [5] and in [6] also predict much larger eccentricity than the Glauber approach. In particular, we shall calculate ε using gluon distributions which account not only for saturation but also for extended geometric scaling (anomalous dimension) and leading-twist shadowing, both of which are important for transverse momenta above the saturation momentum Q_s . We also provide a simple qualitative explanation of the large eccentricity in the CGC approach which motivates that it does not originate from pure “edge effects”. We therefore expect that both the large eccentricity of the transverse overlap region as well as the in-plane “twist” of produced gluons [8] are rather generic predictions of the k_\perp -factorization approach. Finally, using a simple model for energy loss induced by the dense medium, we show how high- p_\perp partons could probe the initial distribution of produced gluons in coordinate space.

II. GLUON PRODUCTION

In the k_\perp -factorization approach the number distribution of produced gluons is given by

$$\frac{dN_g}{d^2r_\perp dy} = \frac{4N_c}{N_c^2 - 1} \int^{p_\perp^{\max}} \frac{d^2p_\perp}{p_\perp^2} \int d^2k_\perp \alpha_s \phi_A(x_1, \mathbf{p}_\perp^2) \times \phi_B(x_2, (\mathbf{p}_\perp - \mathbf{k}_\perp)^2), \quad (2)$$

with $N_c = 3$ the number of colors. Here, p_\perp and y denote the transverse momentum and the rapidity of the produced gluons, respectively. The light-cone momentum fractions of the colliding gluon ladders are then given by $x_{1,2} = p_\perp \exp(\pm y)/\sqrt{s_{NN}}$, where $\sqrt{s_{NN}}$ denotes the center of mass energy. We set p_\perp^{\max} such that the minimal saturation scale $Q_s^{\min}(x_i)$ in the above integration is $\Lambda_{QCD} = 0.2$ GeV. We note that the eccentricity at midrapidity is rather insensitive to the choice of p_\perp^{\max} [9]. The KLN approach [5] employs the following unintegrated gluon distribution function at $x \ll 1$:

$$\phi(x, k_\perp^2; \mathbf{r}_\perp) \sim \frac{1}{\alpha_s(Q_s^2)} \frac{Q_s^2}{\max(Q_s^2, k_\perp^2)}. \quad (3)$$

Q_s denotes the saturation momentum at the given momentum fraction x and transverse position \mathbf{r}_\perp . The overall normalization of ϕ is determined by the multiplicity at midrapidity for the most central collisions. The saturation scale for a nucleus in $A+B$ collisions is then parameterized as

$$Q_s^2(x, \mathbf{r}_\perp) = 2 \text{ GeV}^2 \left(\frac{n_{\text{part}}(\mathbf{r}_\perp)}{1.53} \right) \left(\frac{0.01}{x} \right)^\lambda, \quad (4)$$

where $n_{\text{part}}(\mathbf{r}_\perp)$ is the transverse density of participants. It is calculated from the thickness functions T_A and T_B :

$$\begin{aligned} n_{\text{part}}^A(\mathbf{r}_\perp) &= T_A(\mathbf{r}_\perp + \mathbf{b}/2) \\ &\times (1 - (1 - \sigma_{NN} T_B(\mathbf{r}_\perp - \mathbf{b}/2)/B)^B). \end{aligned} \quad (5)$$

$\mathbf{b} = (b, 0)$ is the impact parameter vector in the transverse plane. The nucleon-nucleon inelastic cross section at $\sqrt{s_{NN}} = 200$ GeV is $\sigma_{NN} = 42$ mb.

The form $Q_s^2(x) \sim x^{-\lambda}$ with $\lambda \approx 0.2 - 0.3$ is motivated by deep inelastic scattering (DIS) data from the Hadron Electron Ring Accelerator (HERA) for $x < 0.01$ [10]. The parameterization (4) leads to an average saturation momentum at midrapidity of about 1.5 GeV for central Au+Au collisions at $\sqrt{s_{NN}} = 200$ GeV, which is in line with standard estimates [5].

The KLN model (3) exhibits a transition from saturation, $\phi(k_\perp^2) \simeq \text{const.}$, directly to the DGLAP regime $\phi(k_\perp^2) \sim 1/k_\perp^2$ at $k_\perp = Q_s$; it does not incorporate leading-twist shadowing since $\phi(k_\perp > Q_s)$ is proportional to the density of participants at a given transverse coordinate. On the other hand, it is well known that DIS data from HERA exhibit approximate “geometric scaling” even for $Q^2 > Q_s^2$ [11]. This indicates that at small x the anomalous dimension $\gamma(k_\perp)$ of the gluon distribution function evolves smoothly towards its DGLAP limit of $\gamma = 1 - \mathcal{O}(\alpha_s) \simeq 1$ as k_\perp/Q_s increases. This is a consequence of quantum evolution of ϕ with $\log 1/x$ [12]. The unintegrated gluon distribution can then be written as

$$\phi(x, k_\perp^2; \mathbf{r}_\perp) \sim \frac{1}{\alpha_s(Q_s^2)} \min \left(1, \left(\frac{Q_s^2}{k_\perp^2} \right)^{\gamma(x, k_\perp^2)} \right). \quad (6)$$

Due to $0 < \gamma < 1$, $\phi(k_\perp^2 > Q_s^2)$ from (6) is harder than the one from the original KLN model. The contribution from the extended geometric scaling regime to the p_\perp -integrated multiplicity is small when Q_s is large. Since the eccentricity ε involves an integration over a wide range of saturation momenta, however, it appears less obvious whether or not the geometric scaling window above Q_s plays a role. Here, we employ the following parameterization of γ for $k_\perp > Q_s$ [13]:

$$\gamma(x_i, k_T^2) = \gamma_s + (1 - \gamma_s) \frac{\log(k_\perp^2/Q_{s,i}^2)}{\lambda Y_i + 1.2\sqrt{Y_i} + \log(k_\perp^2/Q_{s,i}^2)}, \quad (7)$$

where $\gamma_s = 0.627$ is the anomalous dimension corresponding to leading-order (LO) BFKL evolution with saturation boundary conditions in the saddle point approximation [12]. The rapidities Y_i of the fusing gluon ladders are related to their momentum fractions x_i by $Y_i = \log(1/x_i)$.

The extended geometric scaling window corresponds to the region of k_\perp where γ evolves from γ_s to ~ 1 . For asymptotically small x , one can neglect the term $\sim \sqrt{Y}$ in (7) and the upper end of the extended geometric scaling window is then given by $Q_{gs}(x) \sim Q_s^2(x)/Q_0$ [12]; for the central region of RHIC collisions, the approach to the DGLAP regime is mainly driven by the subasymptotic $\sim \sqrt{Y}$ term. The above form of γ reproduces the evolution of inclusive p_\perp -distributions from minimum-bias $d + Au$ collisions with rapidity rather well [13].

Finally, we shall also compute ε using an unintegrated gluon distribution obtained from an *Ansatz* for the dipole forward scattering amplitude [14]:

$$\phi(x, k_\perp^2; \mathbf{r}_\perp) \sim \frac{1}{\alpha_s} \int d^2 \mathbf{u}_\perp e^{-i \mathbf{k}_\perp \cdot \mathbf{u}_\perp} \nabla_\perp^2 N(x, \mathbf{u}_\perp), \quad (8)$$

where \mathbf{u}_\perp is the transverse size of the dipole, conjugate to \mathbf{k}_\perp . A viable model for the unitarized dipole profile is [13, 14]

$$N(x, \mathbf{u}_\perp) = 1 - \exp \left[-\frac{1}{4} (u_\perp^2 Q_s^2)^{\gamma(x, u_\perp^2)} \right]. \quad (9)$$

where the anomalous dimension $\gamma(x, u_\perp^2)$ is of the same form as (7) but with the replacement $k_\perp^2 \rightarrow 1/u_\perp^2$. This dipole profile describes the transitions from saturation ($N(u_\perp) \sim 1$) to the leading-twist extended geometric scaling ($N(u_\perp) \sim (u_\perp^2 Q_s^2)^\gamma$) and DGLAP regimes ($N(u_\perp) \sim u_\perp^2 Q_s^2$). Leading-twist shadowing is present in the extended geometric scaling window since with $Q_s^2 \sim A^{1/3}$, $N \sim A^{\gamma/3}$ exhibits a weaker dependence on the nuclear thickness.

III. RESULTS

In this section, we show the results of a numerical integration of eq. (2), using the above-mentioned models for the unintegrated gluon distribution $\phi(x, k_\perp)$. We shall

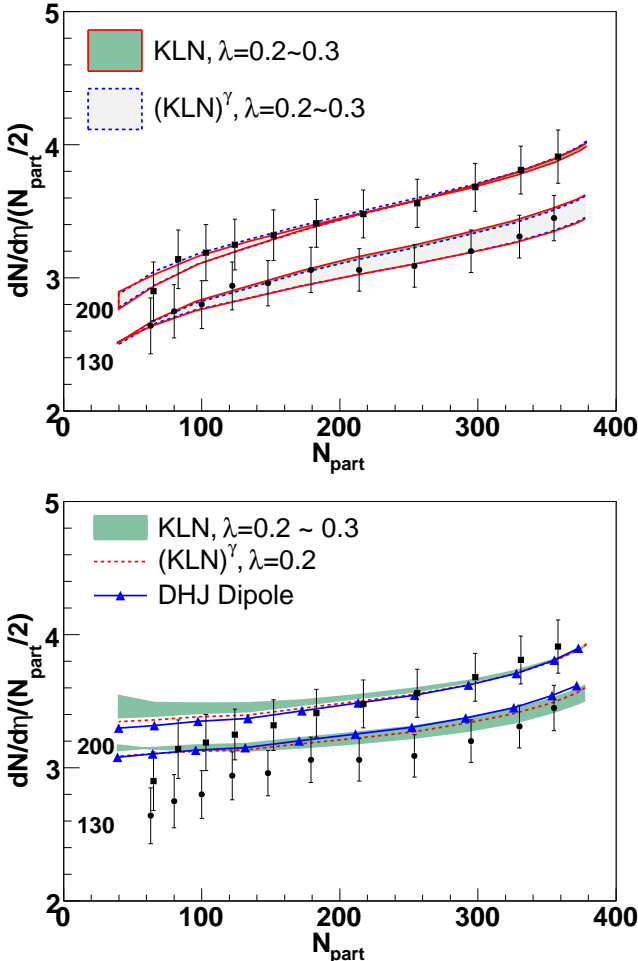


FIG. 1: Centrality dependence of the multiplicity in Au+Au collisions as compared to PHOBOS data [16] for $\sqrt{s_{NN}} = 130$ and 200 GeV. Running (fixed) coupling is used in the upper (lower) panel. λ denotes the growth rate of the saturation momentum with $\log 1/x$. The curves correspond to various parameterizations of the unintegrated gluon distribution function, see text for detailed explanations.

employ both fixed ($\alpha_s = 0.5$) and LO running coupling constants, $\alpha_s(Q_s^2) = 4\pi/9 \log(Q_s^2/\Lambda_{QCD}^2)$ [15].

We first check the centrality dependence of the multiplicity. In Fig. 1 we compare the calculated number of gluons to PHOBOS data [16] for charged hadrons, assuming that the hadron yield is proportional to the yield of produced gluons. “(KLN)” denotes the original KLN parameterization of the unintegrated gluon distribution function (3), “(KLN) $^\gamma$ ” its extension from eq. (6) to include the smooth transition of the anomalous dimension and leading-twist shadowing, and “DHJ Dipole” the unitarized dipole profile from eqs. (8,9). We find that all models are consistent with the data within error bars. As a side-remark, we note that the explicit numerical integration of eq. (2) over \mathbf{r}_\perp improves the KLN results at midrapidity, especially in the high N_{part} region, as com-

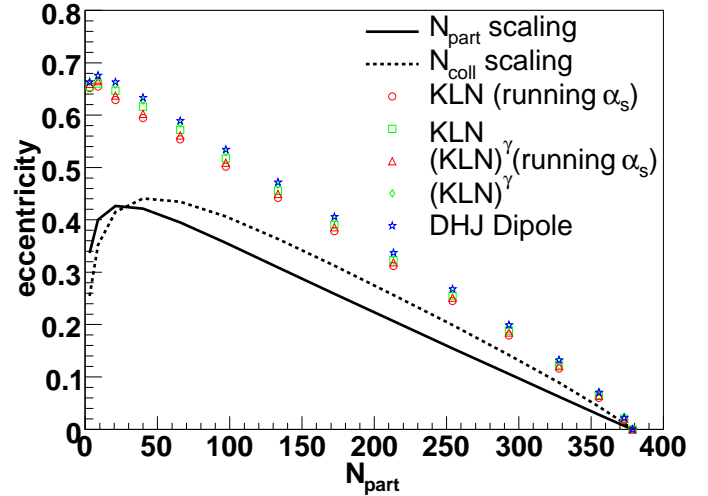


FIG. 2: Initial spatial eccentricity ε at midrapidity as a function of the number of participants for 200 A GeV Au+Au collisions from various models. For comparison, we also show initial conditions where the initial parton density at midrapidity scales with the transverse density of wounded nucleons (full line) and of binary collisions (dotted line) [17].

pared to the $Q_s^2(\mathbf{r}_\perp) \rightarrow \langle Q_s^2 \rangle$ approximation employed in Refs. [5]. We refer to Ref. [9] for a nice explanation of the positive slope of the curve.

Next, in Fig. 2, we compare the eccentricity for the above-mentioned unintegrated gluon distribution functions. Regardless of running or fixed coupling, all saturation models yield almost the same ε as a function of centrality while that predicted by Glauber-type models is much lower. The latter is commonly used as initial condition for hydrodynamical simulations [17], assuming that the energy density in the transverse plane scales with either the number of participants or the number of collisions (dominance of hard processes), respectively. The fact that all of the above models for ϕ predict about the same ε already indicates that the large anisotropy in coordinate space might be generic to the k_\perp -factorization formula (2).

The large predicted eccentricity could be understood qualitatively in the following way. In the k_\perp -factorization approach the number of produced gluons scales approximately with the *smaller* of the saturation scales of the two nuclei [5]. This is valid not only as a function of rapidity but also as a function of the transverse coordinate:

$$\frac{dN}{d^2\mathbf{r}_\perp dy} \sim \min(Q_{s,1}^2(y, \mathbf{r}_\perp), Q_{s,2}^2(y, \mathbf{r}_\perp)). \quad (10)$$

(The transverse energy density $dE_\perp/d^2\mathbf{r}_\perp dy$ in fact involves another factor of Q_s but this is inessential for the present discussion.) To understand this, approximate the local unintegrated gluon distribution by $\phi_A(k_\perp) \simeq \Theta(Q_{s,\min} - k_\perp)$. Scaling with $Q_{s,\min}$ follows also from analytical solutions of the classical Yang-Mills equations

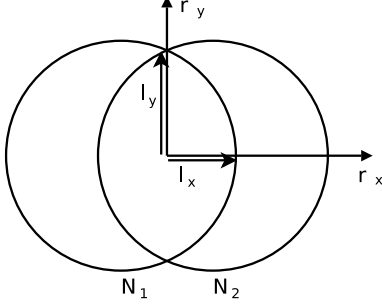


FIG. 3: Along the line \vec{l}_x , the density of gluons in the CGC case falls off more rapidly than in Glauber type models. Along \vec{l}_y , the collision is symmetric and the CGC gluon density behaves similar to the Glauber model. See text for explanation.

for asymmetric collisions [18].

Fig. 3 depicts two paths away from the center of the overlap region. Along \vec{l}_x the number density scales, to logarithmic accuracy, as

$$\rho_{\text{CGC}}(r_x, 0) \sim Q_{s,1}^2(r_x, 0) \sim n_{\text{part},1}(r_x, 0). \quad (11)$$

On the other hand, in the opposite direction along $-\vec{l}_x$ we have

$$\rho_{\text{CGC}}(r_x, 0) \sim Q_{s,2}^2(r_x, 0) \sim n_{\text{part},2}(r_x, 0). \quad (12)$$

In the wounded nucleon model, the density scales with the *total* number of participants from both nuclei,

$$\rho_{\text{Glauber}}(r_x, 0) \sim n_{\text{part},1}(r_x, 0) + n_{\text{part},2}(r_x, 0), \quad (13)$$

which of course drops less rapidly with r_x since the drop of the density towards the edge of the more dilute nucleus is at least partly compensated by the increasing number of participants from the other nucleus.

Along the line $\pm \vec{l}_y$, in turn, both saturation scales are equal and so

$$\begin{aligned} \rho_{\text{CGC}}(0, r_y) &\sim (n_{\text{part},1}(0, r_y) + n_{\text{part},2}(0, r_y))/2 \\ &\sim \rho_{\text{Glauber}}(0, r_y). \end{aligned} \quad (14)$$

Since the number density along l_y drops more rapidly for the CGC initial conditions than for the Glauber model, while both behave the same along l_x , the resulting eccentricity is higher for the former. Thus, the large eccentricity is a feature inherent to the k_\perp -factorization formula.

Contrary to simple geometrical overlap models, the CGC also predicts a non-trivial longitudinal structure of the initial condition. Even under the simplest assumption of *local* quantum evolution, which implies that the \mathbf{r}_\perp -dependence of ϕ arises exclusively via $Q_s^2(x, \mathbf{r}_\perp) \sim n_{\text{part}}(\mathbf{r}_\perp)$ at any rapidity, moments of the density of produced gluons in coordinate space do depend on y ! For example, the “center of gravity” $\langle r_x \rangle$ does not vanish at $y \neq 0$, as already discussed in [8].

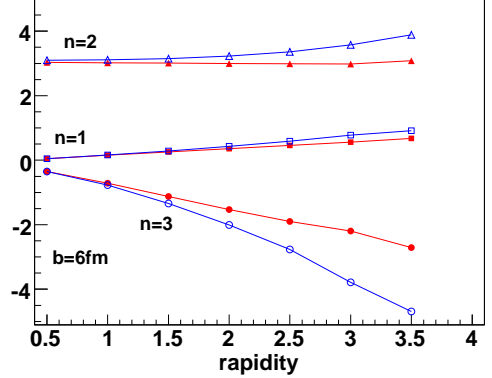


FIG. 4: Moments $\langle (r_x - \langle r_x \rangle)^n \rangle$ (in fm^n) of the coordinate-space distribution of produced gluons as a function of rapidity. Open (closed) symbols correspond to the *Ansatz* (3) with (without) the additional factor of $(1 - x)^4$. The $n = 1, 3$ moments have been scaled up by a factor of 10.

For gluon production at non-zero rapidity the momentum fraction x of one of the fusing gluon ladders grows like $\sim \exp(y)$. In the KLN approach, large- x effects are incorporated into the unintegrated gluon distribution by the substitution $\phi(x, k_\perp^2) \rightarrow \phi(x, k_\perp^2)(1 - x)^4$. This is, of course, a rather qualitative model of large- x effects which does not treat their Q^2 dependence etc.

Fig. 4 shows the evolution of various moments of the energy density of produced gluons with rapidity. The longitudinal structure is clearly non-trivial since odd moments of r_x no longer vanish at $y \neq 0$. Hydrodynamical solutions will exhibit a “left-right” asymmetry (i.e. $v_1 \neq 0$) due to the fact that $\langle (r_x - \langle r_x \rangle)^3 \rangle \neq 0$ [19]. Hence, as compared to the geometry at $y = 0$ illustrated in Fig. 3, not only does the center of the “overlap” shift with rapidity but the entire shape changes. Fig. 4 also shows that the $(1 - x)^4$ factor, which models large- x effects, strongly affects the third moment of r_x at $y \gtrsim 2$. (Other “details” such as p_\perp^{\max} from eq. (2) are also much more important at large y , which is another reason why the numbers from Fig. 4 can not be trusted quantitatively.) This result indicates that our present limited understanding of “large- x ” effects within the CGC formalism inhibits more quantitative calculations of the initial conditions for hydrodynamic models over a broad range of y [20]. In order to compute the observable momentum-space distributions of particles from these initial conditions one needs to solve for the subsequent thermalization and three-dimensional hydrodynamical expansion [21] of produced gluons, which is beyond the scope of the present note.

However, high- p_\perp particles may probe the initial density distribution via final-state interactions such as energy loss. We employ a simple model for radiative energy loss of fast partons to illustrate the qualitative effect.

In a dense QCD medium the induced radiative energy loss reduces the initial transverse momentum p_\perp^0 of

a produced hard parton prior to its fragmentation into hadrons. The “quenching factor” $(1 - \mu\chi)$ depends in general on the initial parton rapidity y , its initial transverse momentum p_\perp^0 as well as on the local density [22]. Here, we consider only mid-rapidity ($y = 0$) partons and further simplify the calculation by neglecting the mild p_\perp dependence of the fractional energy loss. We use the model proposed in [23] and further developed in [24]. μ is a parameter set to reproduce the observed average jet quenching at $b = 0$. For eikonal (straight-line) jet trajectories, the opacity χ of the medium is a function of the initial production point \mathbf{r}_\perp of the jet and of its azimuthal direction of propagation $\hat{\mathbf{v}}_\perp = (\cos \varphi, \sin \varphi)$,

$$\chi(\mathbf{r}_\perp, \hat{\mathbf{v}}_\perp; b) = l_0 \int_{l_0}^{\infty} dl \frac{l - l_0}{l} \rho(\mathbf{r}_\perp + l\hat{\mathbf{v}}_\perp; b). \quad (15)$$

where $\rho(\mathbf{r}_\perp, b)$ denotes the local bulk density. Here, we assume a formation time of the medium of $l_0 = 0.2$ fm. Larger formation times tend to increase the final azimuthal asymmetry [25]. Eq. (15) accounts for non-dissipative one-dimensional expansion of the medium along the beam axis.

For simplicity, we approximate the initial p_\perp -distribution of hard partons with $p_\perp^0 > Q_{gs}$ by a power law $d\sigma/d^2p_\perp^0 dy \sim (p_\perp^0)^{-n(p_\perp^0)}$, where $n(p_\perp^0)$ is a slowly varying function which we calculate in the DGLAP leading-twist approximation. This is justified since, by definition, the anomalous dimension $\gamma \rightarrow \gamma_{\text{DGLAP}}$ in the high- p_\perp regime. The final transverse momentum of a given parton then is $p_\perp = p_\perp^0(1 - \mu\chi)$. We define the quantity $R_{AA}(p_\perp, \varphi; b)$ as the ratio of the initial to the final transverse momentum distributions, omitting fragmentation into hadrons:

$$R_{AA}(p_\perp, \varphi; b) = \left\langle f_g(p_\perp)(1 - \mu\chi)^{n_g(p_\perp) - 2} + (1 - f_g(p_\perp))(1 - \frac{4}{9}\mu\chi)^{n_q(p_\perp) - 2} \right\rangle, \quad (16)$$

where $f_g(p_\perp)$ is the fraction of gluons and $n_{q/g}(p_\perp)$ are the quark and gluon power laws, respectively [26]. The color factor $C_F/C_A = (N^2 - 1)/(2N^2) = 4/9$ accounts for the weaker coupling of quark jets to the medium. The average in (16) is performed over the initial production points \mathbf{r}_\perp of the jets. In the DGLAP regime, these are distributed according to the local number of binary collisions, $\sim T_A(\mathbf{r}_\perp + \mathbf{b}/2) T_B(\mathbf{r}_\perp - \mathbf{b}/2)$.

Fig. 5 displays the angular average $R_{AA}(p_\perp; b)$ of (16) as well as its second harmonic, denoted as $v_2(p_\perp; b)$. The former is rather insensitive to the shape of the “overlap” region as it involves an integral over the azimuth φ . The asymmetry v_2 for semi-central collisions is slightly larger for CGC versus Glauber initial conditions. Nevertheless, for the assumed non-dissipative expansion, which leads to a rather rapid cooling of the medium, the difference is moderate.

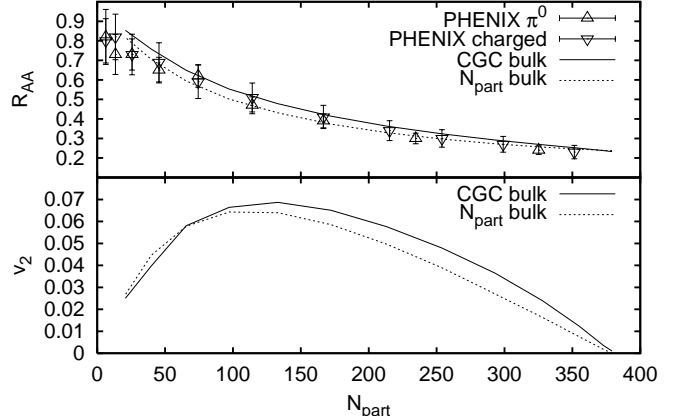


FIG. 5: Top: suppression factor $R_{AA}(p_\perp; b)$ at $p_\perp \simeq 10$ GeV as a function of centrality for CGC/KLN and $\sim N_{\text{part}}$ bulk density distributions, respectively. PHENIX data [27] correspond to hadron transverse momenta $p_\perp > 4.5$ GeV. Bottom: second harmonic coefficient of $R_{AA}(p_\perp, \varphi; b)/R_{AA}(p_\perp; b)$.

IV. CONCLUSIONS

We have shown that the eccentricity predicted by CGC models is larger than that from Glauber models. This property is due to the different scaling behavior of the density in the transverse plane of the collision. Namely, k_\perp -factorization predicts that dN/d^2r_\perp is proportional to the smaller rather than to the average of the two local saturation scales. We also find that the centrality dependence of the multiplicity and of the eccentricity depend only weakly on “details” of the unintegrated gluon distribution function, such as leading-twist shadowing and the anomalous dimension. The centrality dependence of the saturation momentum can be tested further by high- p_\perp particle production in p+A collisions [28].

These observations could be very important for our understanding of the collective expansion of the high-density matter created at RHIC and, in the near future, at the LHC. Larger initial eccentricity should lead to larger v_2 in the final state unless the build-up of azimuthally asymmetric collective flow is damped by dissipative effects. Ref. [6] found that dissipation in the hadronic stage might not be sufficient to explain experimental data. Dissipative corrections to relativistic ideal fluid expansion of a QGP have recently been discussed in refs. [29]. Previous parton cascade simulations with only elastic two-body scattering concluded that a huge transport opacity (large parton cross sections and/or large parton densities) is needed to account for the measured v_2 [30]. It will be most interesting to reconsider those results using the CGC initial conditions suggested here together with parton multiplication processes [31].

Finally, we point out that a better understanding of *large-x* effects within the CGC is important to pro-

vide quantitative results on the structure in coordinate space of the initial condition for hydrodynamic models of heavy-ion collisions at RHIC and LHC.

Acknowledgments

Y. N. acknowledges support from GSI and DFG. H. J. D. is supported by the BMBF-Forschungsvorhaben

05-CU5RI1/3. A. A. thanks S. Wicks and W. Horowitz for useful discussions on energy loss.

[1] J. Y. Ollitrault, Phys. Rev. D **46**, 229 (1992).

[2] B. B. Back *et al.* [PHOBOS Collaboration], Nucl. Phys. A **757**, 28 (2005) [arXiv:nucl-ex/0410022]; J. Adams *et al.* [STAR Collaboration], Nucl. Phys. A **757**, 102 (2005) [arXiv:nucl-ex/0501009]; K. Adcox *et al.* [PHENIX Collaboration], Nucl. Phys. A **757**, 184 (2005) [arXiv:nucl-ex/0410003].

[3] for recent reviews see T. Hirano, Acta Phys. Polon. B **36**, 187 (2005) [arXiv:nucl-th/0410017]; U. W. Heinz, arXiv:nucl-th/0512051; which offer a good introduction to the extensive original literature.

[4] M. Bleicher and H. Stöcker, Phys. Lett. B **526**, 309 (2002) [arXiv:hep-ph/0006147]; X. Zhu, M. Bleicher and H. Stöcker, Phys. Rev. C **72**, 064911 (2005) [arXiv:nucl-th/0509081].

[5] D. Kharzeev and M. Nardi, Phys. Lett. B **507**, 121 (2001) [arXiv:nucl-th/0012025]; D. Kharzeev, E. Levin and M. Nardi, Nucl. Phys. A **730**, 448 (2004) [Erratum-ibid. A **743**, 329 (2004)] [arXiv:hep-ph/0212316]; Nucl. Phys. A **747**, 609 (2005) [arXiv:hep-ph/0408050].

[6] T. Hirano, U. W. Heinz, D. Kharzeev, R. Lacey and Y. Nara, Phys. Lett. B **636**, 299 (2006).

[7] Y. Nara, N. Otuka, A. Ohnishi, K. Niita and S. Chiba, Phys. Rev. C **61**, 024901 (2000) [arXiv:nucl-th/9904059].

[8] A. Adil, M. Gyulassy and T. Hirano, Phys. Rev. D **73**, 074006 (2006) [arXiv:nucl-th/0509064].

[9] A. Kuhlman, U. W. Heinz and Y. V. Kovchegov, nucl-th/0604038.

[10] K. Golec-Biernat and M. Wusthoff, Phys. Rev. D **59**, 014017 (1999) [arXiv:hep-ph/9807513]; Phys. Rev. D **60**, 114023 (1999) [arXiv:hep-ph/9903358].

[11] A. M. Stasto, K. Golec-Biernat and J. Kwiecinski, Phys. Rev. Lett. **86**, 596 (2001) [arXiv:hep-ph/0007192].

[12] E. Levin and K. Tuchin, Nucl. Phys. A **691**, 779 (2001) [arXiv:hep-ph/0012167]; E. Iancu, K. Itakura and L. McLerran, Nucl. Phys. A **708**, 327 (2002) [arXiv:hep-ph/0203137]; Nucl. Phys. A **724**, 181 (2003) [arXiv:hep-ph/0212123]; A. H. Mueller and D. N. Triantafyllopoulos, Nucl. Phys. B **640**, 331 (2002) [arXiv:hep-ph/0205167]; E. Iancu, K. Itakura and S. Munier, Phys. Lett. B **590**, 199 (2004) [arXiv:hep-ph/0310338].

[13] A. Dumitru, A. Hayashigaki and J. Jalilian-Marian, Nucl. Phys. A **765**, 464 (2006) [arXiv:hep-ph/0506308]; Nucl. Phys. A **770**, 57 (2006) [arXiv:hep-ph/0512129].

[14] D. Kharzeev, Y. V. Kovchegov and K. Tuchin, Phys. Rev. D **68**, 094013 (2003) [arXiv:hep-ph/0307037].

[15] A fixed coupling constant can always be absorbed into the overall normalization of the unintegrated gluon distribution and therefore plays no role for the present purpose. For running coupling, we freeze $\alpha_s(Q^2)$ at 0.5 in the low- Q^2 region, as also done in [6, 8]. We have checked that the eccentricity is insensitive to variations of α_s^{\max} by $\pm 50\%$.

[16] B. B. Back *et al.* [PHOBOS Collaboration], Phys. Rev. C **65**, 061901 (2002) [arXiv:nucl-ex/0201005].

[17] P. F. Kolb, U. W. Heinz, P. Huovinen, K. J. Eskola and K. Tuominen, Nucl. Phys. A **696**, 197 (2001) [arXiv:hep-ph/0103234].

[18] A. Dumitru and L. D. McLerran, Nucl. Phys. A **700**, 492 (2002) [arXiv:hep-ph/0105268]; A. Dumitru and J. Jalilian-Marian, Phys. Lett. B **547**, 15 (2002) [arXiv:hep-ph/0111357]; J. P. Blaizot, F. Gelis and R. Venugopalan, Nucl. Phys. A **743**, 13 (2004) [arXiv:hep-ph/0402256].

[19] For lower energies, this has been discussed already, within a different framework, by J. Brachmann *et al.*, Phys. Rev. C **61**, 024909 (2000) [arXiv:nucl-th/9908010].

[20] The situation is different for the forward region of $p + A$ collisions where it is possible to treat the proton within full DGLAP [13], which respects the momentum sum rule and accounts for Q^2 -dependent large- x effects.

[21] T. Hirano and Y. Nara, Nucl. Phys. A **743**, 305 (2004) [arXiv:nucl-th/0404039].

[22] M. Gyulassy, I. Vitev, X. N. Wang and B. W. Zhang, arXiv:nucl-th/0302077; A. Adil and M. Gyulassy, Phys. Lett. B **602**, 52 (2004) [arXiv:nucl-th/0405036].

[23] A. Drees, H. Feng and J. Jia, Phys. Rev. C **71**, 034909 (2005) [arXiv:nucl-th/0310044].

[24] W. A. Horowitz, arXiv:nucl-th/0511052.

[25] V. S. Pantuev, arXiv:hep-ph/0506095; arXiv:hep-ph/0509207.

[26] Strictly speaking, eq. (16) is valid only when $n_g = n_q$. For $n_g - n_q \equiv \delta n \neq 0$ but small ($\delta n \log p_\perp \ll 1$) a correction factor of $1 - (1 - f_g) \delta n \log p_\perp$ appears on the r.h.s. of that equation. Here, we focus on the sensitivity of R_{AA} to the shape of the bulk in the transverse plane at fixed p_\perp ; we therefore absorb this factor into the overall normalization, which is set to reproduce $R_{AA} \approx 0.2$ for the most central collisions.

[27] S. S. Adler *et al.* [PHENIX Collaboration], Phys. Rev. C **69**, 034910 (2004) [arXiv:nucl-ex/0308006].

[28] A. Dumitru, Y. Mehtar-Tani and D. Schiff: in preparation.

[29] A. Muronga, Phys. Rev. Lett. **88**, 062302 (2002) [Erratum-ibid. **89**, 159901 (2002)] [arXiv:nucl-th/0104064]; Phys. Rev. C **69**, 034903 (2004) [arXiv:nucl-th/0309055]; A. Muronga and D. H. Rischke, arXiv:nucl-th/0407114; R. S. Bhalerao, J. P. Blaizot, N. Borghini and J. Y. Ollitrault, Phys. Lett. B **627**, 49 (2005) [arXiv:nucl-th/0508009]; U. W. Heinz, H. Song and A. K. Chaudhuri, Phys. Rev. C **73**, 034904 (2006)

[arXiv:nucl-th/0510014]; R. Baier, P. Romatschke and U. A. Wiedemann, hep-ph/0602249; nucl-th/0604006; K. Paech and S. Pratt, nucl-th/0604008.

[30] D. Molnar and M. Gyulassy, Nucl. Phys. A **697**, 495 (2002) [Erratum-ibid. A **703**, 893 (2002)] [arXiv:nucl-th/0104073].

[31] Z. Xu and C. Greiner, Phys. Rev. C **71**, 064901 (2005) [arXiv:hep-ph/0406278]; hep-ph/0509324.

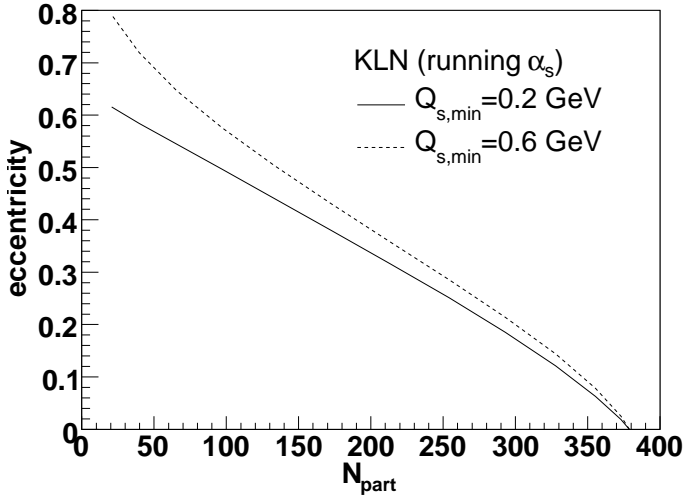


FIG. 6: **Additional Figure:** Eccentricity as a function of N_{part} for the KLN-model of the unintegrated gluon distribution function. The cut-off in the integrations over k_{\perp} and p_{\perp} in eq. (2) is varied from our “standard” choice of $Q_s(x_i) > \Lambda_{\text{QCD}}$ to $Q_s(x_i) > 3\Lambda_{\text{QCD}}$. Note that a larger cut-off effectively chops off part of the low-density rim of the “overlap” region. The eccentricity then increases slightly.

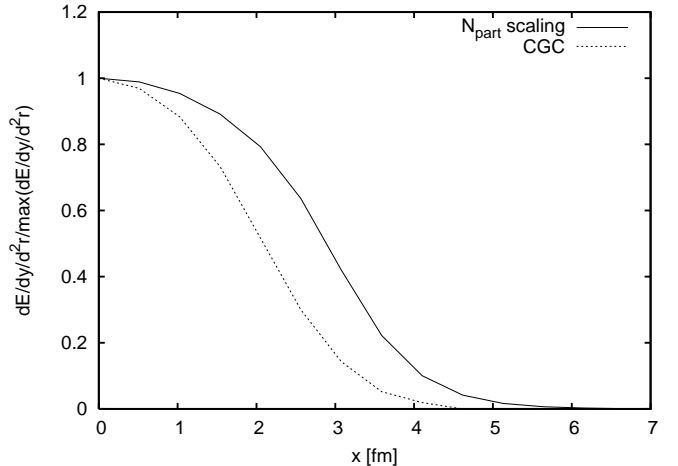


FIG. 7: **Additional Figure:** The mid-rapidity energy density profile for a Au+Au collision at $b = 8$ fm as obtained from eq. (2) with the KLN unintegrated gluon distribution or from a Glauber model, respectively.